Radiotherapy and Oncology 141 (2019) 200–207

Contents lists available at ScienceDirect

Radiotherapy and Oncology

journal homepage: www.thegreenjournal.com

Original Article

End-to-end empirical validation of dose accumulation in MRI-guided adaptive radiotherapy for prostate cancer using an anthropomorphic deformable pelvis phantom

Omar Bohoudi [a,*], Frank J. Lagerwaard [a], Anna M.E. Bruynzeel [a], Nina I. Niebuhr [b,c,d], Wibke Johnen [b,c], Suresh Senan [a], Ben J. Slotman [a], Asja Pfaffenberger [b,c], Miguel A. Palacios [a]

[a] Dept. Of Radiation Oncology, Amsterdam University Medical Centers, location VUmc, The Netherlands; [b] Medical Physics in Radiation Oncology, German Cancer Research Center DKFZ; [c] Heidelberg Institute for Radiation Oncology (HIRO), National Center for Radiation Research in Oncology (NCRO); and [d] Department of Physics and Astronomy, Heidelberg University, Heidelberg, Germany

ARTICLE INFO

Article history:
Received 14 June 2019
Received in revised form 12 September 2019
Accepted 14 September 2019
Available online 1 October 2019

Keywords:
MR-guided
MRgRT
Adaptive
Prostate cancer
Dose accumulation
Deformable image registration

ABSTRACT

Background and purpose: This work evaluates the accuracy of deformable dose accumulation for organs at risk (OAR) in MR-guided prostate SBRT using an anthropomorphic deformable phantom.

Materials and methods: Six MR-guided prostate SBRT treatment courses were simulated using volumetric OAR (bladder and rectum) information derived from actual patient data. Deformed OAR contours, geometrical landmarks and GafChromic EBT3 film strips ($1.25 \times 2.0\ cm^2$) placed at the surface of the OARs were used to validate DIR-based dose accumulation in MRgRT. Two DIR methods were applied: an intensity-based deformation (IB-D) applied to the whole image, and a contour-based deformation (CB-D), resulting in a separate deformation and dose accumulation for each OAR.

Dosimetric accuracy was evaluated by quantifying the dose differences, and performing a gamma-index analysis between measured and DIR-derived accumulated dose for both OARs. Geometrical accuracy was assessed by measuring the Dice similarity coefficient (DSC), Hausdorff distance (HDD) and residual distance error (RDE) for all markers at each fraction.

Results: CB-D resulted in an average dose deviation from film measurements for rectum and bladder surfaces of 0.6% and 0.3%, respectively. IB-D led to worse results resulting in an overall average dose accumulation inaccuracy of 7.2% and 2.5% for rectum and bladder. CB-D also showed a higher geometrical accuracy than IB-D with significantly higher DSC values and lower RDE and HDD deviations.

Conclusion: Empirical validation of dose accumulation in MR-guided SBRT for prostate cancer obtained a good agreement with reference film measurements when using a contour-based DIR approach.

In-room image-guidance has become a cornerstone in radiotherapy, both for assessing inter-fractional anatomical changes and performing adaptive radiotherapy (ART) [1,2]. The position and shape of target and critical organs may vary during the course of radiotherapy and, in the absence of online plan adaptation, can lead to differences between the planned and the actual delivered dose distribution [3,4]. Recently, the potential of MR-guided radiotherapy (MRgRT) for better visualization of inter-fractional anatomical changes and online plan adaptation in prostate cancer has been appraised [5,6]. Besides online plan adaptation, knowledge of the inter-fractional changes that have taken place has also drawn interest towards the evaluation of the accumulated dose received by the target and critical organs during the course of the treatment [7–9].

For an accurate determination of the cumulative total dose delivered to the target volume and organs at risk (OAR), dose accumulation over all fractions is required. Deformable image registration (DIR) allows voxel-to-voxel mapping between a baseline reference image (MRI or CT) and subsequent images of deformed tissues. Application of the deformation map to the dose distribution enables dose warping from all fractions to the reference image and estimation of the total received dose. For this reason, DIR-based dose accumulation methods have been developed and explored during the last years [10–13]. However, performance evaluation and estimation of the uncertainty in the accumulated dose is essential prior to clinical implementation [7,14], especially in the regions of high dose gradients, where small errors in the deformation map can result in significant changes in the accumu-

* Corresponding author at: Amsterdam University Medical Center, location VUmc, Postbox 7057, 1007 MB Amsterdam, The Netherlands.
E-mail address: o.bohoudi@amsterdamumc.nl (O. Bohoudi).

https://doi.org/10.1016/j.radonc.2019.09.014
0167-8140/

lated dose. This might be the case, for instance, with the dose received by the rectum and bladder across all fractions in prostate radiotherapy.

Anthropomorphic phantoms are valuable tools for the performance evaluation of DIR-based dose accumulation because they can be used for evaluating the entire process, including image acquisition with possible distortion and noise, data transfer and import, image registration and dose delivery [14]. The phantom needs to represent the anatomy of a patient, be equipped with realistic organ densities visually distinguishable by the image modality being employed and finally, be able to accommodate suitable dosimeters and geometrical landmarks in clinically relevant locations. These phantoms should also offer controllable motion and deformation, be able to reproduce different clinical situations and suitable to perform reference measurements for DIR evaluation [14].

In the past, validations of dose accumulation using CBCT images of (numerical) phantoms were performed [15–21], but thus far no empirical validation of dose accumulation for online adaptive MRgRT has been reported. MRgRT introduces possible sources of error such as spatial distortion of MR images, use of deformed electron density for dose calculation and variability in intensity levels of MR images. An end-to-end test of dose accumulation performance under these conditions is essential prior to clinical use.

Several groups have reported on DIR-based dose accumulation in actual patients [16,22–25], but there is a lack of studies in the literature validating DIR-based dose accumulation over a radiotherapy treatment course involving realistic clinical situations. In this study, such a validation for dose accumulation in MRgRT is presented. For this purpose, an anthropomorphic, deformable and multimodal phantom of the male pelvis was used [26] to simulate actual clinical situations derived from previously treated patients. Six stereotactic body radiotherapy (SBRT) treatment courses for prostate cancer were simulated using all five fractions, and the accuracy of the final accumulated dose in critical organs assessed using GafChromic EBT3 film dosimetry.

Materials and methods

Phantom specification

The ADAM-pelvis phantom, an Anthropomorphic, Deformable And Multimodal phantom developed in the German Cancer Research Center (DKFZ), was used in this study (Fig. 1a). The construction and specification of this phantom is described in greater detail by Niebuhr et al. [26–28]. Briefly, in the engineering of this pelvis phantom, agarose gels loaded with sodium fluoride and a Gadolinium-based contrast agent were used for multimodal simulation of soft tissue, whereas vegetable oils were used to mimic adipose tissue. Simulation of pelvic bones was realized by applying gypsum bandage and Vaseline to a 3D printed hollow bone case, resulting in both a fatty bone marrow signal in MRI and high- and low attenuation areas in CT scans. The prostate-, bladder- and rectum surrogates were cast using 3D printed molds generated from real patient-data. These organ surrogates were manufactured of silicone to allow controllable and reproducible organ motion and deformation, enabling simulation of various realistic MR-guided adaptive radiation delivery scenarios. Imaging marker points and pockets for dosimeters were implemented into the surfaces of these organ surrogates to serve as a geometric and dosimetric reference in the evaluation of geometric DIR and dose accumulation accuracy. Dosimetric evaluation was performed using GafChromic EBT3 films, which has been reported to be suitable and shown high accuracy in the presence of a 0.35 T magnetic field [29]. Custom-fit film strips ($1.25 \times 2.0\ cm^2$) were inserted in seven bladder and two rectum surface pockets (Fig. 1b and c) to evaluate the dose to critical structures.

MRgRT simulation

Six patients with prostate cancer who previously underwent MRgRT treatments with online plan adaption, delivered in five fractions on the MRIdian system (ViewRay Inc., Mountain View, USA), were simulated on this phantom (TX_{PAT}). The bladder volumes and consistency of the rectum filling (air or "substance", simulated with sponge (water/dry)) were varied before each simulated fraction, based on available patient imaging data to create realistic organ deformation scenarios. At each fraction, an MR scan (TR/TE: 3.37 ms/1.45 ms; FA: 60°) with 1.5 mm × 1.5 mm × 1.5 mm resolution was performed on the phantom. Dose prescriptions delivered for the actual treatment (5×7.25 Gy) were rescaled to 5×2 Gy in order to remain in the best dose range performance of GafChromic EBT3 films (0.2–10 Gy). Baseline treatment plans were generated using IMRT step-and-shoot with 5 beam groups where each beam group had three equidistant beams corresponding with three ^{60}Co sources on the gantry. Dose calculation at each fraction was performed with a Monte-Carlo algorithm (statistical uncertainty of 1%) with a grid resolution of 0.3 cm × 0.3 cm × 0.3 cm using the deformed electron density map from the simulation CT scan.

The same procedures as in the clinical setting were followed for daily online plan adaptation for each TX_{PAT} (see also Fig. 1, Supplementary material): (1) A repeat MR scan for each fraction, followed by 3D alignment of the baseline and repeat MR-scan based on the CTV; (2) Automatic deformation of OAR contours; and (3) Plan re-optimization using the same beam numbers, beam directions and optimization objectives.

For each TX_{PAT} the EBT3 film strips remained in the same pockets indicated in Fig. 1 keeping identical orientation during all 5 delivered fractions, in order to measure the cumulative delivered dose and to serve as benchmark for assessing the accuracy DIR-based dose accumulation. At the end of each TX_{PAT} (after 5 fractions) the irradiated EBT3 film strips were taken out and stored in light-shielding bags. After 24 h each filmstrip was digitized according to the procedure described by Barten et al. [29].

DIR algorithm and dose accumulation

For each $TX_{PAT,}$ the acquired 3D MR scan, contours and dose distribution were imported into the publicly available open-source software 3DSlicer (v4.10.0) [30]. Elastix, an intensity-based DIR toolkit available through the SlicerElastix extension, was used for voxel-to-voxel mapping between the reference image (MRI fraction 1; MR_{REF}) and subsequent images (MR fraction 2–5; $MR_{FR2\text{-}5}$) [31,32]. DIR parameters used in this study were a normalized mutual information similarity metric with a B-spline parameterized transformation. Furthermore, a three-level multiresolution registration scheme was used with image resolution and grid spacing down sampled by a factor of 2 at each multiresolution level, and final B-spline grid spacing of 10 mm. Gradient descent optimization was used with up to 500 iterations at each multiresolution level.

Two different DIR approaches were assessed for each TX_{PAT} (Fig. 2): (1) full image DIR approach (IB-D), were a voxel-to-voxel mapping between the ***entire*** MR_{REF} and the ***entire*** MR_{FR2} to MR_{FR5} was established, resulting in 4 consecutive deformation vector fields for each subsequent fraction of TX_{PAT} ($DVF^{FX2\text{-}5}$); (2) contour–guided DIR approach (CB-D), were a separate bladder- and rectum-specific voxel-to-voxel mapping is established between MR_{REF} and $MR_{FR2\text{-}5}$, resulting in 4 consecutive DVF for the bladder ($DVF^{FR2\text{-}5}_{(bladder)}$) and 4 consecutive DVF for the rectum ($DVF^{FX2\text{-}5}_{(rectum)}$).

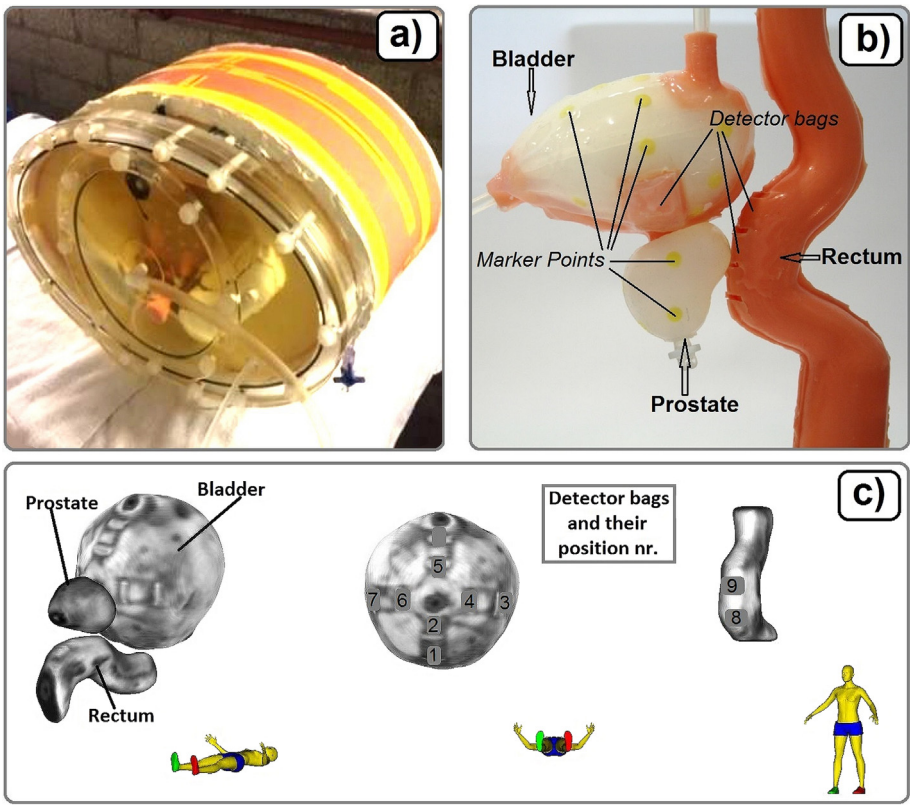

Fig. 1. Illustration of the ADAM deformable pelvic phantom (a), and corresponding image of organ surrogates including imaging marker points and pockets for dosimeters (b). The lower panel (c) shows an MRI surface plot of the bladder, prostate and rectum of the phantom. The positions of the detector bags for film strips are numbered from 1 to 9.

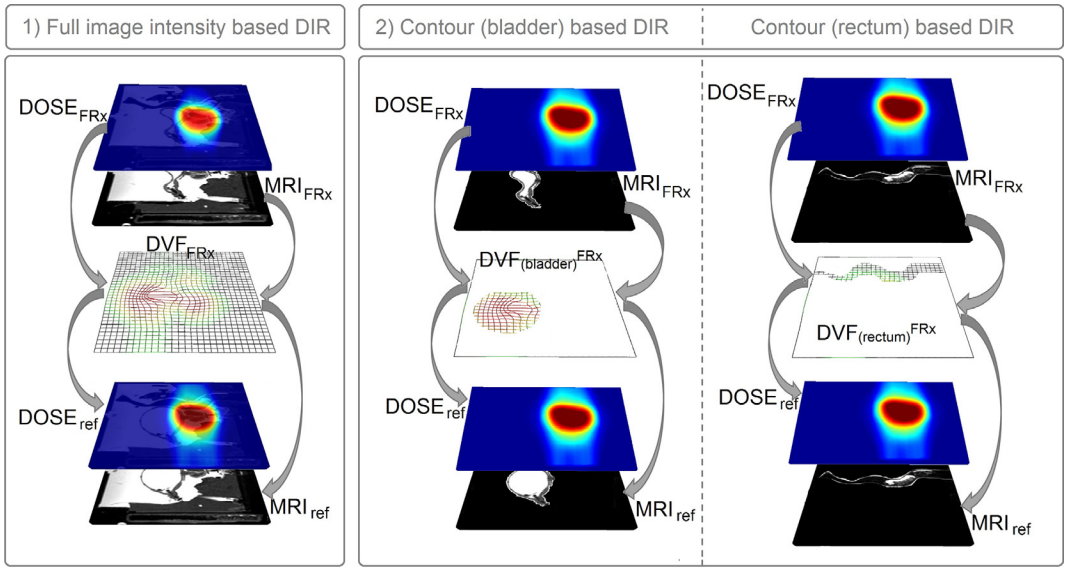

Fig. 2. Schematic illustration demonstrating the workflow for both DIR approaches.

With the CB-D approach the DIR is thus constrained to the volume encompassed by the respective OAR contour, i.e. bladder or rectum. MR images used as input for both IB-D and CB-D approaches were previously registered to the CTV of the pre-treatment image during the online adaptive workflow (see also, Supplementary material and [5,33]).

The $DVF^{FX2\text{-}5}$ from the IB-D approach were applied to the dose distributions of fractions 2, 3, 4 and 5 respectively, in order to map the dose distributions at each fraction to the dose distribution of fraction 1 (reference image, MR_{REF}). Finally, the warped dose distributions were summed up to obtain the total accumulated dose for each TX_{PAT}. For the second DIR approach CB-D, a bladder- and rectum-specific accumulated dose was obtained using the $DVF_{(rectum/bladder)}{}^{FX2\text{-}5}$ after following the same procedure for each organ separately.

Dosimetric and geometric evaluation of DIR

To evaluate the DIR-based dose accumulation accuracy, the exact location of all EBT3 films strips on MR_{REF} were identified

and marked with a ROI in Slicer for each treatment simulation (see also Fig. 2, suppl. material). The accumulated dose distribution within these ROIs after applying both methods, IB-D and CB-D, were extracted and exported from Slicer in the same format (tiff) as the digitalized EBT3 filmstrips. A pixel-by-pixel analysis of the calibrated filmstrips (dose readout) and the extracted ROIs with the accumulated doses was performed using OmniPo-I'mRT v.1.7 software (IBA Dosimetry, Schwarzenbruck) (Fig. 3, supplementary material). A correction for the dose contribution from the simulation CT carried out at baseline was performed by adding a constant absolute dose value to each pixel in the ROIs containing the accumulated dose distribution (see also Supplementary material). Relative dose difference calculations across all pixels in the films ($\Delta DOSE_{(\%)} = 100\% * (Dose_{(EBT3)}/DOSE_{(DIR)})$) were performed to evaluate the dosimetric accuracy of both DIR strategies, IB-D and CB-D. In addition, the accumulated spatial dose distributions of TX_{PAT1-6} were further evaluated using the gamma index (3%/2 mm) for all film strips [34].

Quantitative evaluation of the geometric DIR accuracy was performed to complement the dose accumulation analysis. Two similarity metrics were used to quantify the organ deformation before and after DIR: Dice similarity coefficient (DSC) [35] and Hausdorff distance (HDD) [36]. The bladder and rectum contour volumes for all TX_{PAT1-6} PRE-DIR, and after IB-D and CB-D strategies were evaluated and compared to the reference contours (MR_{FX1}). Sixteen marker points available on the surface of the bladder and rectum were identified on each MRI to generate a reference position for each fraction. A total of 56 and 8 marker data points were generated per TX_{PAT} over the 4 fractions for the bladder and rectum, respectively. The marker points defined on MR_{FR2-5} were propagated to MR_{REF} using the relevant DVFs. The geometric accuracy of DIR was evaluated by calculating the Euclidean distance (residual distance error, RDE) between the propagated and reference marker point locations.

Statistical analysis comparing both DIR approaches was performed using the Wilcoxon Signed-Rank test (IBM® SPSS Statistics v20, Armonk, NY, USA). A p-value <0.05 was considered to be statistically significant.

Results

Fig. 3 shows a 3D representation of the simulated treatments and OAR inter-fractional changes in the anthropomorphic pelvis phantom. Variations in bladder and rectum volume were substantial reflecting different anatomical situations at each fraction. Fig. 4 reports on the DSC, HDD and changes in bladder and rectum volume with respect to the MR_{REF} before applying DIR (PRE-DIR).

Fig. 3. An overview of 3D recreations of the prostate, rectum and bladder on the ADAM-pelvis phantom for all fractions of the six simulated SBRT prostate treatments (TX_{PAT1-6}). The MR anatomical scan of the ADAM-pelvis phantom is shown for the reference situation. Bladder at each fraction is depicted in green whereas the rectum is depicted in blue. Densities in rectum were variable according to the simulated clinical data. Baseline anatomy for the OAR is represented at each fraction with translucent structures to show inter-fractional anatomical changes.

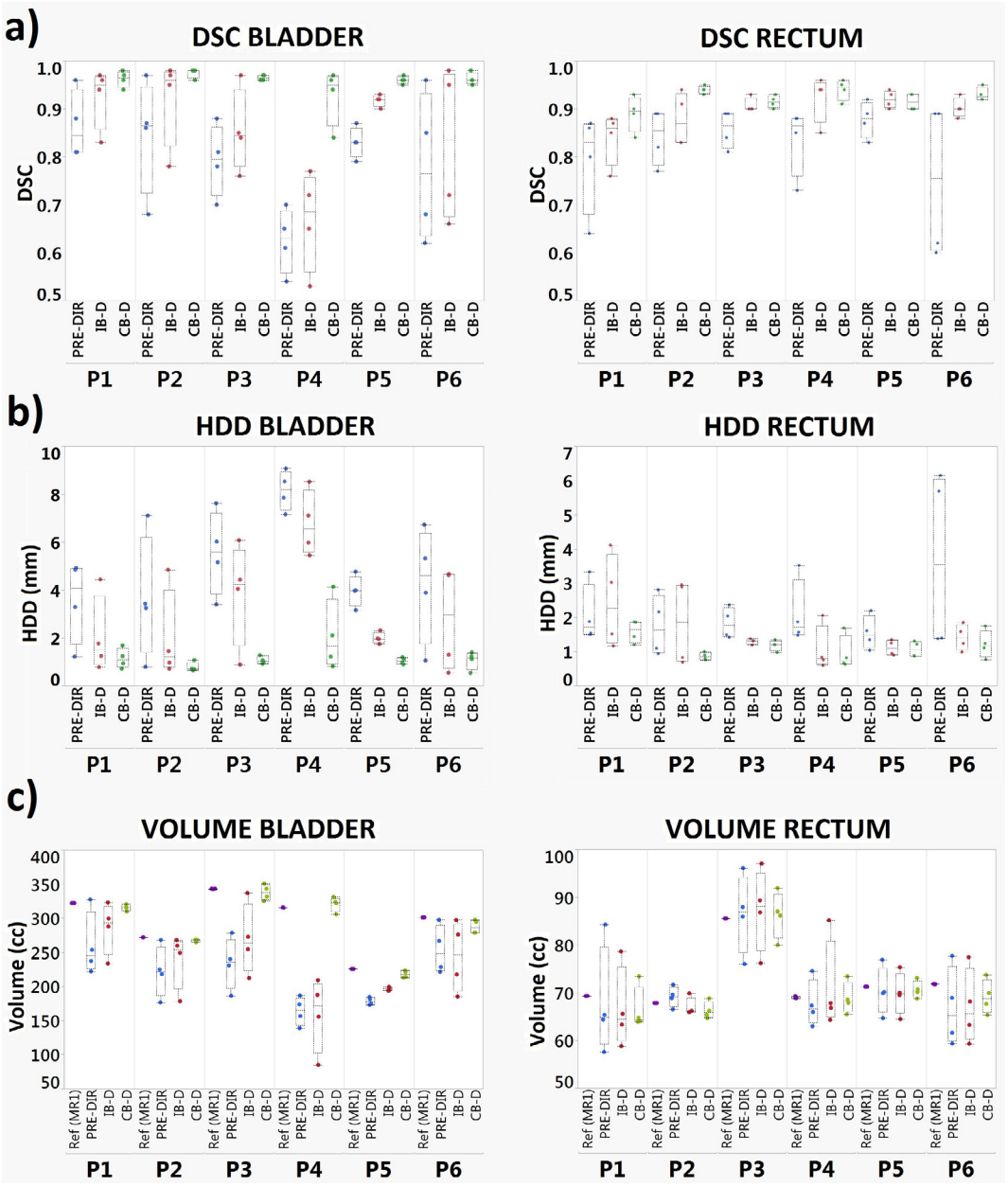

Fig. 4. The DSC, HDD and volumes of bladder and rectum changes with respect to MR_{REF} before (PRE-DIR) applying DIR and after IB-D and CB-D strategies.

Dosimetric accuracy of DIR

Both IB-D and CB-D dose accumulation approaches were carried out for all TX_{PAT}. A detailed overview of the $\Delta DOSE_{(\%)}$ for both IB-D and CB-D with respect to the dose readout of the films located at the bladder- and rectum surfaces is shown in Table 1. An excellent agreement with the measured values was achieved by CB-D, whereas the IB-D approach resulted in large deviations for several patients. Overall the mean $\Delta DOSE_{(\%)}$ averaged over all pixels for all TX_{PAT} showed a relative dose difference of 2.5% (SD = 8.7) and −0.6% (SD = 2.0) at the bladder surface, and 7.2% (SD = 10.9) and 0.3% (SD = 1.3) at the rectum surface for IB-D and CB-D, respectively. The higher correspondence of CB-D with the reference film measurements was significant for both bladder surface ($p = 0.024$) and rectum surface ($p = 0.033$). Analysis of gamma pass rates between the film dose readouts and the accumulated doses by IB-D and CB-D are also listed in Table 1. CB-D dose accumulation resulted in high gamma pass rates values for all TX_{PAT} whereas IB-D exhibited significant lower values and clearly underperformed for several TX_{PAT}.

Geometric accuracy of DIR

Similar to the dosimetric results, CB-D turned out to be superior to IB-D and achieved a higher accuracy to represent the actual geometry at each fraction. The mean bladder DSC and HDD after IB-D registration over all TX_{PAT1-6} was 0.85 (SD = 0.12) and 3.18 mm (SD = 2.27), respectively. CB-D resulted in an improved DIR registration for the bladder with DSC and HDD mean values of 0.96 (SD = 0.03) and 1.20 mm (SD = 0.70), respectively ($p < 0.001$, $p < 0.001$). Likewise, IB-D resulted in an inferior registration than CB-D for the rectum, with mean values of DSC and HDD of 0.89 (SD = 0.04) and 1.53 mm (SD = 0.86) vs 0.93 (SD = 0.03) and 1.15 mm (SD = 0.36) ($p < 0.001$, $p = 0.025$). The obtained bladder and rectum contour volumes for all TX_{PAT1-6} after IB-D and CB-D

Table 1
Relative dose difference and gamma (3%/2 mm) pass-rates for both dose accumulation methods with respect to the film dose readouts at the bladder- and rectum surface in TX_{PAT1} to TX_{PAT6}.

		ΔDOSE (%)		gamma pass rate % ($\gamma < 1$) (3%/2 mm)	
		IB-DIR	CB-DIR	IB- DIR	CB-DIR
TX_{PAT1}	Bladder	1.3 ± 1.2	−0.7 ± 1.0	97.1	98.6
	Rectum	25.7 ± 11.3	0.4 ± 0.5	45.0	99.0
TX_{PAT2}	Bladder	0.9 ± 5.9	−2.2 ± 1.7	75.3	92.4
	Rectum	8.9 ± 0.9	0.1 ± 0.4	51.8	98.2
TX_{PAT3}	Bladder	−3.3 ± 5.2	0.3 ± 2.1	83.6	93.9
	Rectum	2.5 ± 3.0	0.7 ± 0.6	81.4	95.3
TX_{PAT4}	Bladder	6.7 ± 6.6	−0.5 ± 1.2	70.6	94.8
	Rectum	4.4 ± 5.6	0.7 ± 1.6	80.8	87.9
TX_{PAT5}	Bladder	2.0 ± 6.4	−0.6 ± 0.9	87.3	96.0
	Rectum	−3.0 ± 1.1	−1.1 ± 0.2	79.8	90.3
TX_{PAT6}	Bladder	7.3 ± 15.1	−0.2 ± 2.9	73.6	91.2
	Rectum	4.6 ± 7.9	1.1 ± 2.2	78.0	91.8

registration in comparison to the reference contours (MR_{REF}) are shown in Fig. 4c. The resulting contour volumes after CB-D showed a higher correspondence than IB-D with the reference contour volumes in all TX_{PAT1-6} for both, bladder and rectum ($r^2 = 0.95$ *vs* 0.37 for bladder, $r^2 = 0.82$ *vs* 0.52 for rectum).

The mean RDE averaged over all bladder imaging marker points was 7.9 mm (SD = 10.6) and 3.3 mm (SD = 3.9) for IB-D and CB-D, respectively (see also Supplementary material). When using CB-D, only TX_{PAT4} led to a deviation larger than 3 mm for the markers located at the bladder surface, whereas all TX_{PAT1-6} for IB-D showed a mean RDE ≥4 mm. For the rectum, the mean RDE was 5.7 mm (SD = 7.7) and 2.5 mm (SD = 2.5) for IB-D and CB-D, respectively. Only TX_{PAT1} and TX_{PAT2} exhibited a mean RDE >3 mm for the rectum imaging markers when using both, IB-D and CB-D approaches. Statistical analysis showed that CB-D exhibited a higher correspondence with the reference marker positions for the bladder ($p = 0.000$) as well as the rectum surface ($p = 0.005$) compared to IB-D.

Discussion

Parallel with the development of recent improvements for in-room image guidance, there has been a growing interest in DIR and dose accumulation for adaptive radiotherapy. Several groups have reported on DIR-based dose accumulation in actual patients [16,22–25], but there is a lack of studies in the literature validating DIR dose accumulation over a radiotherapy treatment course involving realistic clinical situations. This study provides such a validation using an anthropomorphic phantom of the human pelvic region to simulate a SBRT prostate cancer treatment course. Our results show an excellent agreement between the accumulated dose and the film measurements after delivery of 5 fractions at the surface of the OARs, i.e. bladder and rectum, especially when using the CB-D approach.

Some previous studies have reported on the accuracy of DIR algorithms for dose accumulation using different classes of deformable phantoms [19,20,37,38]. In contrast to the present study, none of those reports simulated an entire MRgRT treatment course using realistic deformations obtained from actual clinical patient data. The performance of such end-to-end tests is a critical component to ensure the accuracy of all steps involved in MRgRT and perform DIR-based dose accumulation. Usually, a single deformation was applied in those studies and the obtained degree of accuracy of the DIR-based dose accumulation was variable, with uncertainties ranging from 1.5 to 4.7%, but with outliers of up to 30%, and mean geometric uncertainties of 1.0–2.1 mm. Our results obtained with the CB-D strategy agreed with the measured doses, with an average deviation of −0.6% and 0.3% for bladder and rectal surfaces, respectively. In addition, the ability to verify the cumulative irradiated dose by means of film dosimetry allowed us to not only estimate the average uncertainty, but also to verify local dose distributions and dose gradients by the gamma index. High gamma pass-rates were obtained for all films measurements with CB-D dose accumulation, whereas performance of IB-D was significantly worse. The mean geometric uncertainties assessed by the CB-D in our study were 3.3 mm and 2.5 mm for the bladder and rectum marker points. Overall, the AAPM recommends an overall DIR geometric accuracy of approximately 2–3 mm [14]. Our results point out that the CB-D method applied accurately predicts the accumulated dose in regions of high dose gradients for patients undergoing substantial deformations and tissue density changes. These results agree with those of Cazoulat et al. [17] who also found that a surface constrained DIR for bladder and rectum using numerical phantoms reduced the local difference between the reference and accumulated doses.

The agreement of the DIR-based accumulated dose with the reference measurements exhibits a correlation with the geometrical error after DIR. Fig. 5 shows the average dose difference for all TX_{PAT1-6} across all fractions plotted against the mean HDD and DSC after DIR. A larger HDD or lower DSC, reflecting a worse correspondence of reference and deformed contour was correlated with a larger average dose difference error. In general, we found that wen using CB-D, HDD distances <3 mm and DSC values >0.90 correlated with dosimetric errors of less than 3% for both, bladder and rectum surfaces. A similar pattern for prostate cancer patients was also found in the past [17].

The anatomical variations in a few SBRT fractions were more difficult to manage by the Elastix DIR algorithm which resulted in higher geometrical uncertainties for both approaches. TX_{PAT4} resulted in >3 mm average marker position deviation from the reference for the bladder surface, and TX_{PAT1-2} for the rectum surface. In the case of TX_{PAT4}, the reference image at baseline showed a full bladder whereas subsequent fractions exhibited a substantial bladder volume decrease, i.e. deformations larger than average were present. For TX_{PAT1-2}, a substantial density change was observed in the voxels comprised by the rectum structure (air vs water equivalent material) in a few fractions, hampering the DIR algorithm to obtain an accurate deformation field locally around the rectum structure. Both extreme situations led to large deviations in the accumulated dose by IB-D, whereas CB-D was still able to accurately accumulate the dose and obtain a good agreement with the experimental measurements. It is worth noting that the largest geometrical deviations found for the bladder reference markers were located cranially, whereas there were no film pockets at those

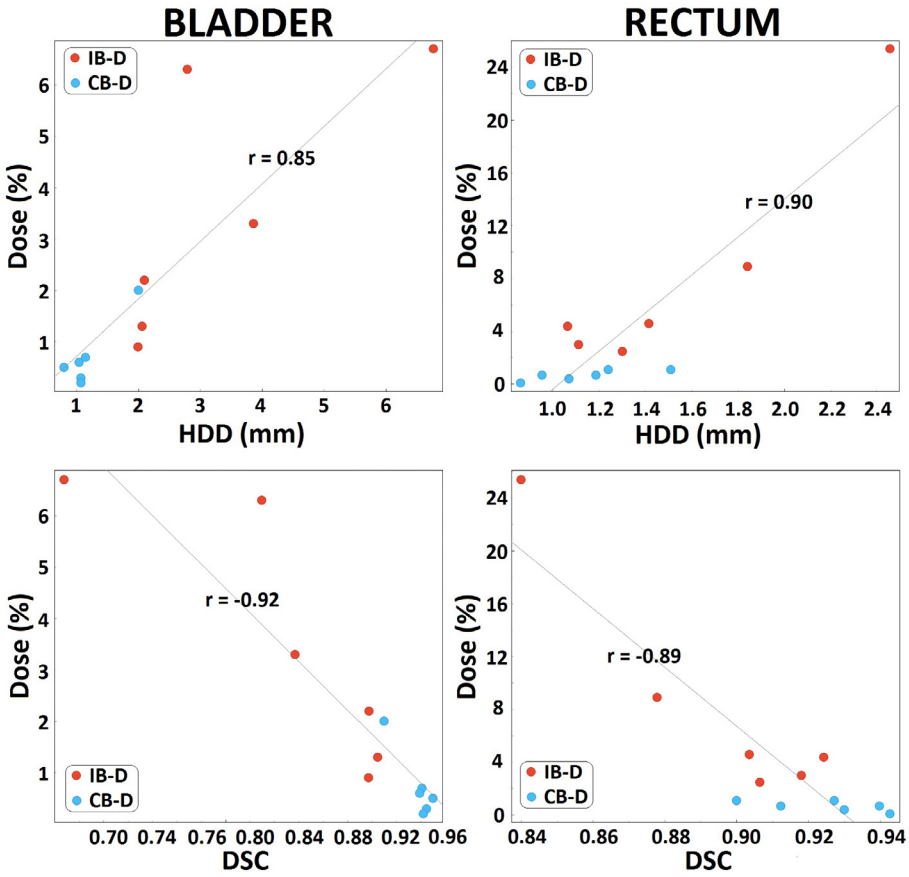

Fig. 5. Mean dose difference for all TX_{PAT1-6} across all fractions plotted against the mean HDD and DSC after applying DIR. Correlation coefficients are shown in the subplots.

locations since they are dosimetrically less relevant (low dose spill).

Our study simulated MR-guided SBRT treatments using actual inter-fractional changes from six prostate cancer patients previously treated in our clinic. MRgRT has shown much potential to improve radiotherapy treatment by means of target volume reduction, online plan adaptation and management of inter-fractional changes [33,39–44]. Validation of DIR dose accumulation in OARs enables future assessment of the received dose by the critical structures and holds much promise for radiotherapy plan adaptation based on the partially received dose at mid-treatment.

Declaration of Competing Interest

The authors declare that they have no known competing financial interests or personal relationships that could have appeared to influence the work reported in this paper.

Acknowledgements

We sincerely thank Marloes Jeulink, Paul van Duijvenvoorde, Daan Hoffmans and Roosje Bakker for their aid during the experimental measurements.

Appendix A. Supplementary data

Supplementary data to this article can be found online at https://doi.org/10.1016/j.radonc.2019.09.014.

References

[1] Wu QJ, Li T, Wu Q, Yin F-F. Adaptive radiation therapy: technical components and clinical applications. Cancer J 2011;17:182–9. https://doi.org/10.1097/PPO.0b013e31821da9d8.
[2] McVicar N, Popescu IA, Heath E. Techniques for adaptive prostate radiotherapy. Phys Medica 2016;32:492–8. https://doi.org/10.1016/j.ejmp.2016.03.010.
[3] Song W, Wong E, Bauman G, Battista J, Van Dyk J. Dosimetric evaluation of daily rigid and non-rigid geometric correction strategies during on-line image-guided radiation therapy (IGRT) of prostate cancer. Med Phys 2007;34:2327–8. https://doi.org/10.1118/1.2760332.
[4] Godley A, Ahunbay E, Peng C, Li XA. Automated registration of large deformations for adaptive radiation therapy of prostate cancer. Med Phys 2009;36:1433–41. https://doi.org/10.1118/1.3095777.
[5] Tetar SU, Bruynzeel AME, Lagerwaard FJ, Slotman BJ, Bohoudi O, Palacios MA. Clinical implementation of magnetic resonance imaging guided adaptive radiotherapy for localized prostate cancer. Phys Imaging Radiat Oncol 2019;9:69–76. https://doi.org/10.1016/j.phro.2019.02.002.
[6] McPartlin AJ, Li XA, Kershaw LE, Heide U, Kerkmeijer L, Lawton C, et al. MRI-guided prostate adaptive radiotherapy – a systematic reviewMRI-linac and prostate motion review. Radiother Oncol 2016;119:371–80. https://doi.org/10.1016/j.radonc.2016.04.014.
[7] Jaffray DA, Lindsay PE, Brock KK, Deasy JO, Tomé WA. Accurate accumulation of dose for improved understanding of radiation effects in normal tissue. Int J Radiat Oncol Biol Phys 2010;76:135–9. https://doi.org/10.1016/j.ijrobp.2009.06.093.
[8] Andersen ES, Muren LP, Sørensen TS, Noe KØ, Thor M, Petersen JB, et al. Bladder dose accumulation based on a biomechanical deformable image registration algorithm in volumetric modulated arc therapy for prostate cancer. Phys Med Biol 2012;57:7089–100. https://doi.org/10.1088/0031-9155/57/21/7089.
[9] Takeda K, Takayama Y, Miyasaka Y, Chiba M, Kadoya N, Sato K, et al. Evaluation of the performance of deformable image registration between planning CT and CBCT images for the pelvic region: comparison between hybrid and intensity-based DIR. J Radiat Res 2017;58:567–71. https://doi.org/10.1093/jrr/rrw123.
[10] Kashani R, Hub M, Balter JM, Kessler ML, Dong L, Zhang L, et al. Objective assessment of deformable image registration in radiotherapy: a multi-institution study. Med Phys 2008;35:5944–53. https://doi.org/10.1118/1.3013563.

[11] Latifi K, Caudell J, Zhang G, Hunt D, Moros EG, Feygelman V. Practical quantification of image registration accuracy following the AAPM TG-132 report framework. J Appl Clin Med Phys 2018;19:125–33. https://doi.org/10.1002/acm2.12348.
[12] Moteabbed M, Sharp GC, Wang Y, Trofimov A, Efstathiou JA, Lu H-M. Validation of a deformable image registration technique for cone beam CT-based dose verification. Med Phys 2014;42:196–205. https://doi.org/10.1118/1.4903292.
[13] Motegi K, Tachibana H, Motegi A, Hotta K, Baba H, Akimoto T. Usefulness of hybrid deformable image registration algorithms in prostate radiation therapy. J Appl Clin Med Phys 2019;20:229–36. https://doi.org/10.1002/acm2.12515.
[14] Brock KK, Mutic S, McNutt TR, Li H, Kessler ML. Use of image registration and fusion algorithms and techniques in radiotherapy: report of the AAPM Radiation Therapy Committee Task Group No. 132: Report. Med Phys 2017;44:e43–76. https://doi.org/10.1002/mp.12256.
[15] Kirby N, Chuang C, Ueda U, Pouliot J, Kirby N, Chuang C, et al. The need for application-based adaptation of deformable image registration. Med Phys 2015:1–10. https://doi.org/10.1118/1.4769114. 011702.
[16] Thor M, Andersen ES, Petersen JBB, Sørensen TS, Noe KØ, Tanderup K, et al. Evaluation of an application for intensity-based deformable image registration and dose accumulation in radiotherapy. Acta Oncol 2014;53:1329–36. https://doi.org/10.3109/0284186X.2014.928742.
[17] Cazoulat G, Simon A, Dumenil A, Gnep K, De Crevoisier R, Acosta O, et al. Surface-constrained nonrigid registration for dose monitoring in prostate cancer radiotherapy. IEEE Trans Med Imaging 2014;33:1464–74. https://doi.org/10.1109/TMI.2014.2314574.
[18] Nassef M, Simon A, Cazoulat G, Duménil A, Blay C, Lafond C, et al. Quantification of dose uncertainties in cumulated dose estimation compared to planned dose in prostate IMRT. Radiother Oncol 2016;119:129–36. https://doi.org/10.1016/j.radonc.2016.03.007.
[19] Graves YJ, Smith AA, McIlvena D, Manilay Z, Lai YK, Rice R, et al. A deformable head and neck phantom with in-vivo dosimetry for adaptive radiotherapy quality assurance. Med Phys 2015;42:1490–7. https://doi.org/10.1118/1.4908205.
[20] Niu CJ, Foltz WD, Velec M, Moseley JL, Al-Mayah A, Brock KK. A novel technique to enable experimental validation of deformable dose accumulation. Med Phys 2012;39:765–76. https://doi.org/10.1118/1.3676185.
[21] Janssens G, de Xivry JO, Fekkes S, Dekker A, Macq B, Lambin P, et al. Evaluation of nonrigid registration models for interfraction dose accumulation in radiotherapy. Med Phys 2009;36:4268–76. https://doi.org/10.1118/1.3194750.
[22] Jamema SV, Mahantshetty U, Andersen E, Noe KT, Sørensen TS, Kallehauge JF, et al. Uncertainties of deformable image registration for dose accumulation of high-dose regions in bladder and rectum in locally advanced cervical cancer. Brachytherapy 2015;14:953–62. https://doi.org/10.1016/j.brachy.2015.08.011.
[23] Kadoya N, Miyasaka YY, Yamamoto T, Kuroda Y, Ito K, Chiba M, et al. Evaluation of rectum and bladder dose accumulation from external beam radiotherapy and brachytherapy for cervical cancer using two different deformable image registration techniques. J Radiat Res 2017;58:720–8. https://doi.org/10.1093/jrr/rrx028.
[24] van Heerden LE, Houweling AC, Koedooder K, van Kesteren Z, van Wieringen N, Rasch CRN, et al. Structure-based deformable image registration: Added value for dose accumulation of external beam radiotherapy and brachytherapy in cervical cancer. Radiother Oncol 2017;123:319–24. https://doi.org/10.1016/j.radonc.2017.03.015.
[25] Vestergaard A, Muren LP, Søndergaard J, Elstrøm UV, Høyer M, Petersen JB. Adaptive plan selection vs. re-optimisation in radiotherapy for bladder cancer: a dose accumulation comparison. Radiother Oncol 2013;109:457–62. https://doi.org/10.1016/j.radonc.2013.08.045.
[26] Niebuhr NI, Johnen W, Echner G, Runz A, Bach M, Stoll M, et al. The ADAM-pelvis phantom – an anthropomorphic, deformable and multimodal phantom for MRgRT. Phys Med Biol 2019. https://doi.org/10.1088/1361-6560/aafd5f. aafd5f.
[27] Niebuhr NI, Johnen W, Güldaglar T, Runz A, Echner G, Mann P, et al. Radiological properties of tissue surrogates used in a multimodality deformable pelvic phantom for MR-guided radiotherapy. Med Phys 2015; accepted f. doi:10.1118/1.4939874.
[28] Johnen W, Niebuhr N, Runz A, Echner G. The ADAM-pelvis phantom: from DICOM data to a patient-like model. Radiother Oncol 2018;127:S930. https://doi.org/10.1016/S0167-8140(18)32046-2.
[29] Barten DLJ, Hoffmans D, Palacios MA, Heukelom S, Van Battum LJ. Suitability of EBT3 GafChromic film for quality assurance in MR-guided radiotherapy at 0.35 T with and without real-time MR imaging. Phys Med Biol 2018;63. https://doi.org/10.1088/1361-6560/aad58d.
[30] Pinter C, Lasso A, Wang A, Jaffray D, Fichtinger G. SlicerRT: radiation therapy research toolkit for 3D Slicer. Med Phys 2012;39:6332–8. https://doi.org/10.1118/1.4754659.
[31] Klein S, Staring M, Murphy K, Viergever MA, Pluim JPW. elastix: a toolbox for intensity-based medical image registration. Med Imaging, IEEE Trans 2010;29:196–205. https://doi.org/10.1109/TMI.2009.2035616.
[32] Marstal K, Berendsen F, ... MS-P of the I, 2016 U. SimpleElastix: A user-friendly, multi-lingual library for medical image registration segmentation sensing unread. IEEE Conf. Comput. Vis. Pattern Recognit. Work., 2016, p. 574–82. doi:10.1109/CVPRW.2016.78.
[33] Bohoudi O, Bruynzeel AME, Senan S, Cuijpers JP, Slotman BJ, Lagerwaard FJ, et al. Fast and robust online adaptive planning in stereotactic MR-guided adaptive radiation therapy (SMART) for pancreatic cancer. Radiother Oncol 2017;125:439–44.
[34] Low DA, Harms WB, Mutic S, Purdy JA. A technique for the quantitative evaluation of dose distributions. Med Phys 1998:656–61.
[35] Dice LR. Measures of the Amount of Ecologic Association Between Species Author (s): Lee R . Dice Published by : Ecological Society of America Stable URL : http://www.jstor.org/stable/1932409 2009;26:297–302.
[36] Dubuisson M, Jain AK, Lansing E, B AB. A Modi ed Hausdor Distance for Object Matching between two point sets A = f 1 compute and does not require the solution of the cor- 1 Introduction two point sets A and B can be combined in the follow- 2 Distance Between Point Sets Research supported by a 1994:566–8.
[37] Janssens G, Orban De Xivry J, Fekkes S, Dekker A, MacQ B, Lambin P, et al. Evaluation of nonrigid registration models for interfraction dose accumulation in radiotherapy. Med Phys 2009;36:4268–76. https://doi.org/10.1118/1.3194750.
[38] Yeo UJ, Taylor ML, Supple JR, Smith RL, Dunn L, Kron T, et al. Is it sensible to "deform" dose? 3D experimental validation of dose-warping. Med Phys 2012;39:5065–72. https://doi.org/10.1118/1.4736534.
[39] Henke L, Kashani R, Robinson C, Curcuru A, DeWees T, Bradley J, et al. Phase I trial of stereotactic MR-guided online adaptive radiation therapy (SMART) for the treatment of oligometastatic or unresectable primary malignancies of the abdomen. Radiother Oncol 2018;126:519–26. https://doi.org/10.1016/J.RADONC.2017.11.032.
[40] Palacios MA, Bohoudi O, Bruynzeel AME, van Sörsen de Koste JR, Cobussen P, Slotman BJ, et al. Role of daily plan adaptation in MR-guided stereotactic ablative radiation therapy for adrenal metastases. Int J Radiat Oncol Biol Phys 2018;102:426–33. https://doi.org/10.1016/j.ijrobp.2018.06.002.
[41] van Sörnsen de Koste JR, Palacios MA, Bruynzeel AME, Slotman BJ, Senan S, Lagerwaard FJ. MR-guided gated stereotactic radiation therapy delivery for lung, adrenal, and pancreatic tumors: a geometric analysis. Int J Radiat Oncol 2018;102:858–66. https://doi.org/10.1016/J.IJROBP.2018.05.048.
[42] Bohoudi O, Bruynzeel AME, Meijerink MR, Senan S, Slotman BJ, Palacios MA, et al. Identification of patients with locally advanced pancreatic cancer benefitting from plan adaptation in MR-guided radiation therapy. Radiother Oncol 2019;132:16–22. https://doi.org/10.1016/j.radonc.2018.11.019.
[43] Fischer-Valuck BW, Henke L, Green O, Kashani R, Acharya S, Bradley JD, et al. Two-and-a-half-year clinical experience with the world's first magnetic resonance image guided radiation therapy system. Adv Radiat Oncol 2017;2:485–93. https://doi.org/10.1016/j.adro.2017.05.006.
[44] Werensteijn-honingh AM, Kroon PS, Winkel D, Aalbers EM, Van Asselen B, Bol GH, et al. Feasibility of stereotactic radiotherapy using a 1. 5 T MR-linac: multi-fraction treatment of pelvic lymph node oligometastases. Radiother Oncol 2019;134:50–4. https://doi.org/10.1016/j.radonc.2019.01.024.